Autoradiographic determination of AGS proton beam-spot size for experiment E951

P.A. Thieberger and H.G. Kirk, Brookhaven National Laboratory

The accurate knowledge of the profile of the 24 GeV AGS proton beam interacting with the experiment E951 targets is critical to evaluate the results in terms of energy densities deposited in mercury and in the various solid materials tested. A fluorescent flag viewed trough a TV camera was used to tune the beam and a digitized image of that beam spot image was at first used to determine the approximate beam size. However the quality of the image wasn't entirely satisfactory, and there also were questions regarding possible saturation of the phosphor which is a problem known to have caused difficulties with similar systems in the past, in particular with such highly intense and concentrated beams. It was therefore decided to investigate the activation pattern of thin windows which had been tested at positions close to the interaction points of the remaining targets. An added benefit expected from this investigation was the verification of the beam-target alignment.

Autoradiographic images of various activated windows were obtained using Polaroid 667 film packs. After ~6 months, the activity of these targets, each of which only saw a few beam pulses, was so weak that one to two week exposures were required to obtain adequate images. The windows were taped to the black exterior paper protecting the negatives as indicated in Fig. 1

Fig.1

For most of the exposures only the first picture was used, and the rest of the film pack was discarded. In one instance all the pictures were kept showing rapid absorption of the radiation indicating that the images are mainly due to β–rays or perhaps very low energy X-rays. These results are discussed towards the end of this note.

In fig. 1 one can see the fiducial marks, both on the targets and on the film-pack, which were used as references to establish the beam spot position with respect to the center of each target. Before developing the picture, the fiducial marks on the film-pack were transferred to the negative by sticking a sharp needle through the black paper at each of those fiducial marks, making small holes in the negative and allowing some light to penetrate to the negative. Before pealing off the positive from the negative, these small holes were further transferred to the positive using the same needle. The resulting Polaroid picture for the case of the 10 mil Havar target is seen in Fig.2

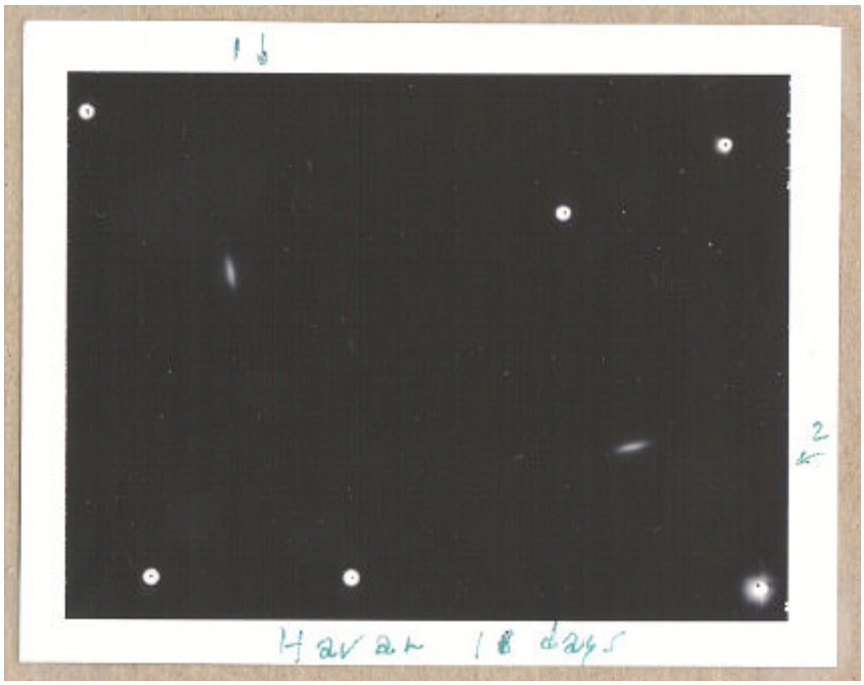

Fig. 2

The negative of such a picture (for the 10 mil Al targets in this case) is shown in Fig. 3 superimposed, by using the fiducial marks, with the image of the targets mounted on the film pack.

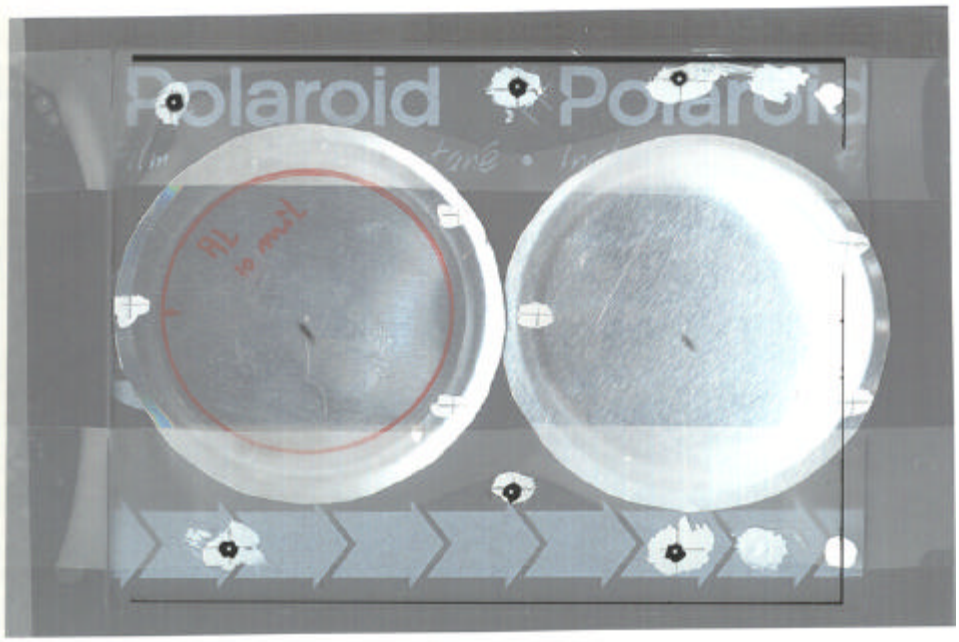

Fig. 3

Each of the superimposed images forming Fig. 3 was obtain by scanning the Polaroid picture and the film-pack with the targets on the same flat-bed scanner to ensure identical scales. From fig. 3 we thus determine that, in this case, the beam was about 3 mm from the center of the 52 mm diameter targets.

Factors potentially affecting the accuracy of the autoradiographic method for determining the beam spot size are the finite target thickness and the distance from the target surface to the negative film.

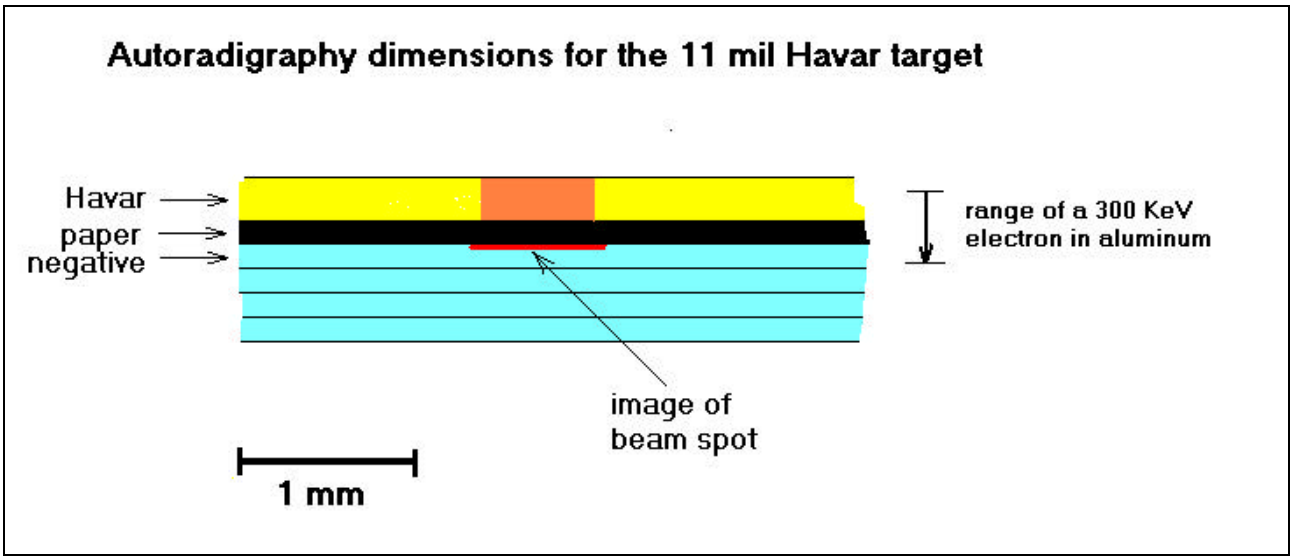

Fig.4

Fig. 4 shows the relative width of the beam-spot compared to the 0.14mm thickness of the negatives, the 0.13mm thickness of the intervening paper and the 0.28 mm target material. We can see that some widening of the image due to this geometry can be expected. A recent measurement of the absorption of the radiation in subsequent negatives (see below) indicates that that the range is considerably smaller than the 300 KeV electron range indicated in the figure. Thus most of the radiation impinging on the negative originates from the lower part of the target and the widening will not be very significant.

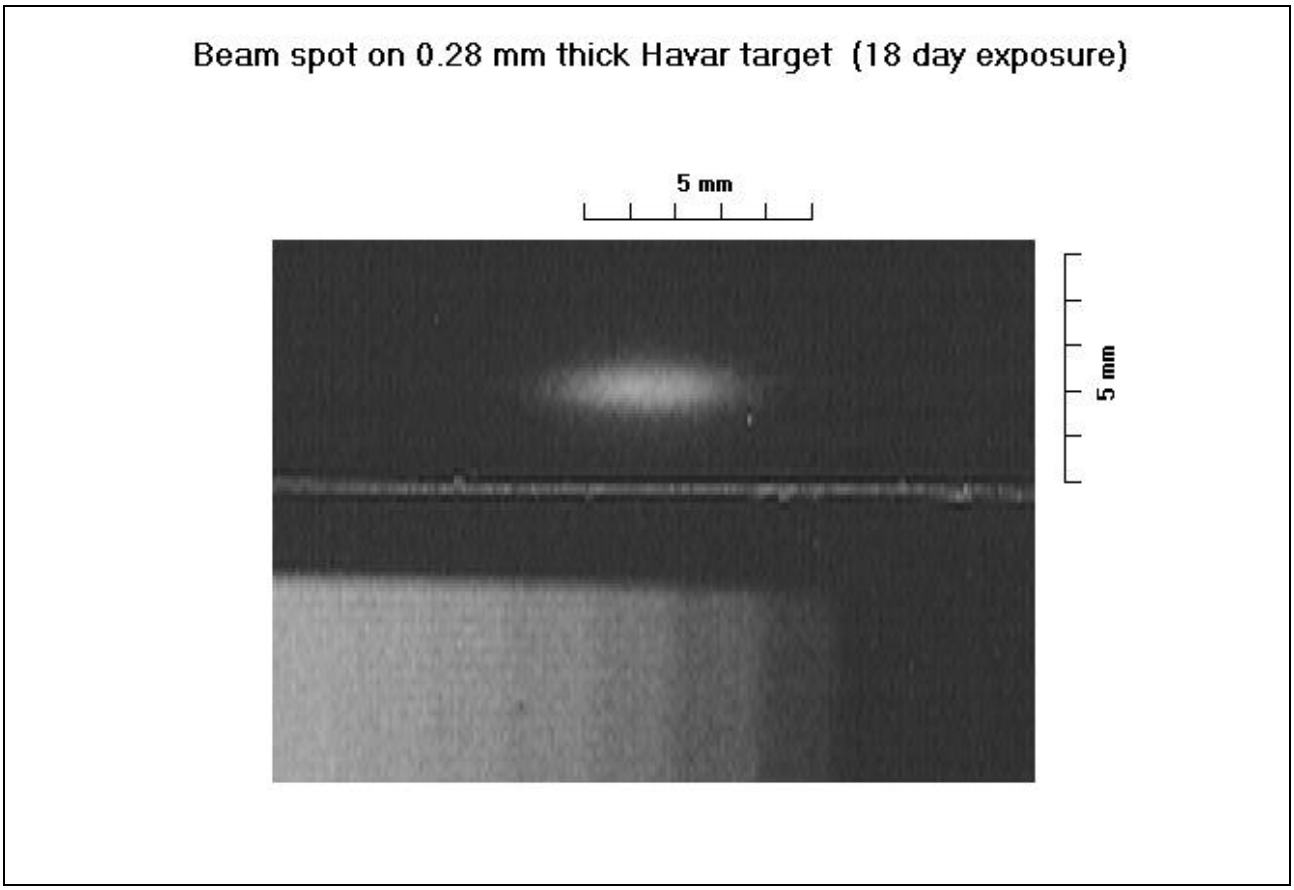

Fig. 5 - Enlarged digitized image of one of the beam spots of fig. 2 together with a calibrating gray-scale (see text).

In order to evaluate the digital data of fig. 5, obtained by scanning the beam-spot image on a flat-bed scanner, one needs to calibrate the combined response of scanner plus film to correlate a measured gray-scale value (0 to 255) of a given point, and the corresponding exposure of the film. To obtain such a gray scale calibration we expose sections of the film to linearly increasing amounts of light obtained with linearly growing light bars on a black computer screen as schematically indicated in Fig.6. In doing this, one needs to defocus the camera to sufficiently blur the image of individual screen pixels. By using the same film and the same scanner to generate this gray-scale one obtains a overall calibration applicable to the beam-spot image. The only assumption is that the non-linearity of the film is the same for visible light than for the measured radiation.

Figure 7 shows the data obtained for this calibration and a polynomial fit used to correct the measured gray-scale values for the beam spot image.

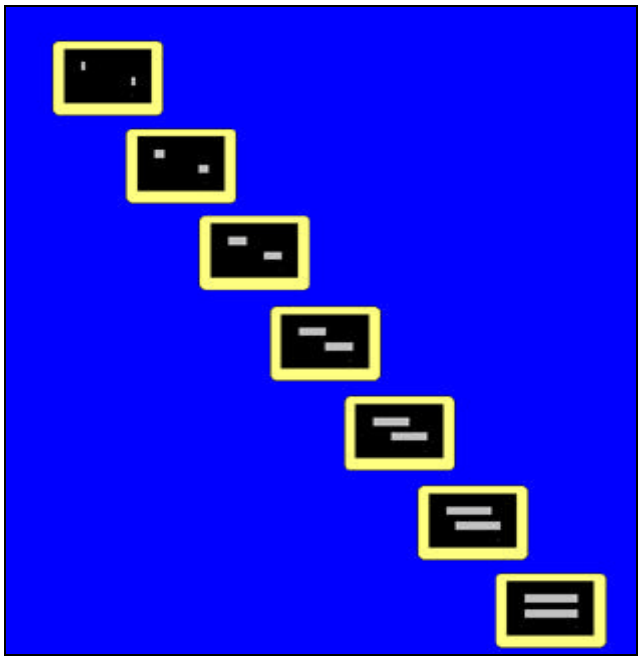

Fig. 6 - Schematic representation of the linearly growing gray bars on a computer screen used for gray-scale calibration. The individual rectangles represent snapshots of the screen with time increasing from left to right.

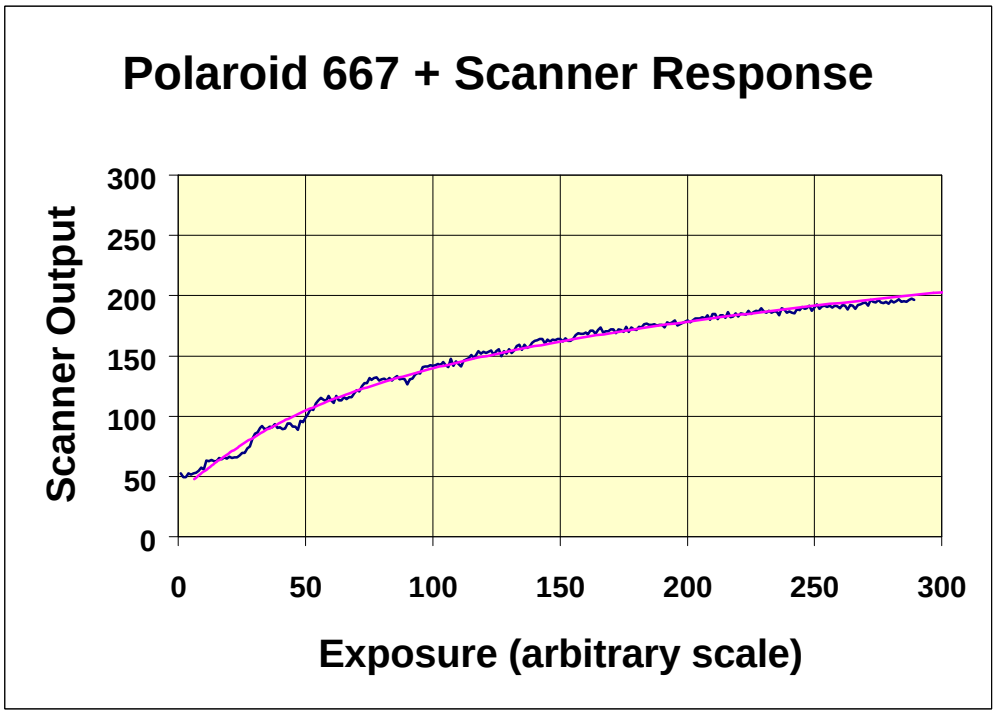

Fig. 7 - Combined gray-scale calibration of film + scanner.

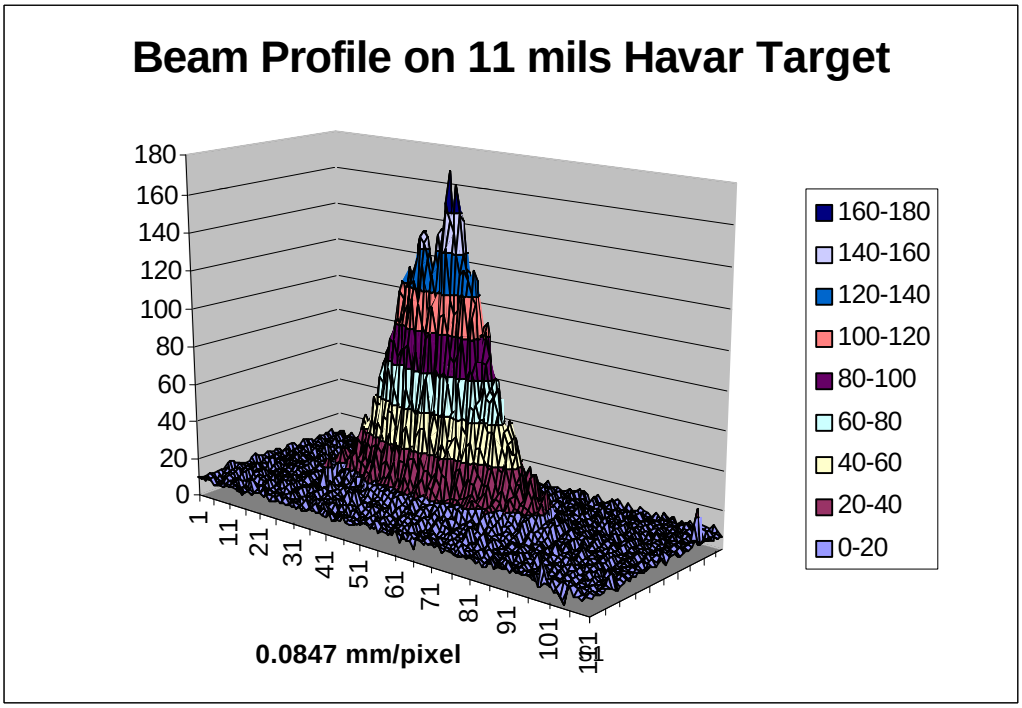

Fig. 8 - Beam spot intensity values obtained after applying the gray-scale calibration of fig.7

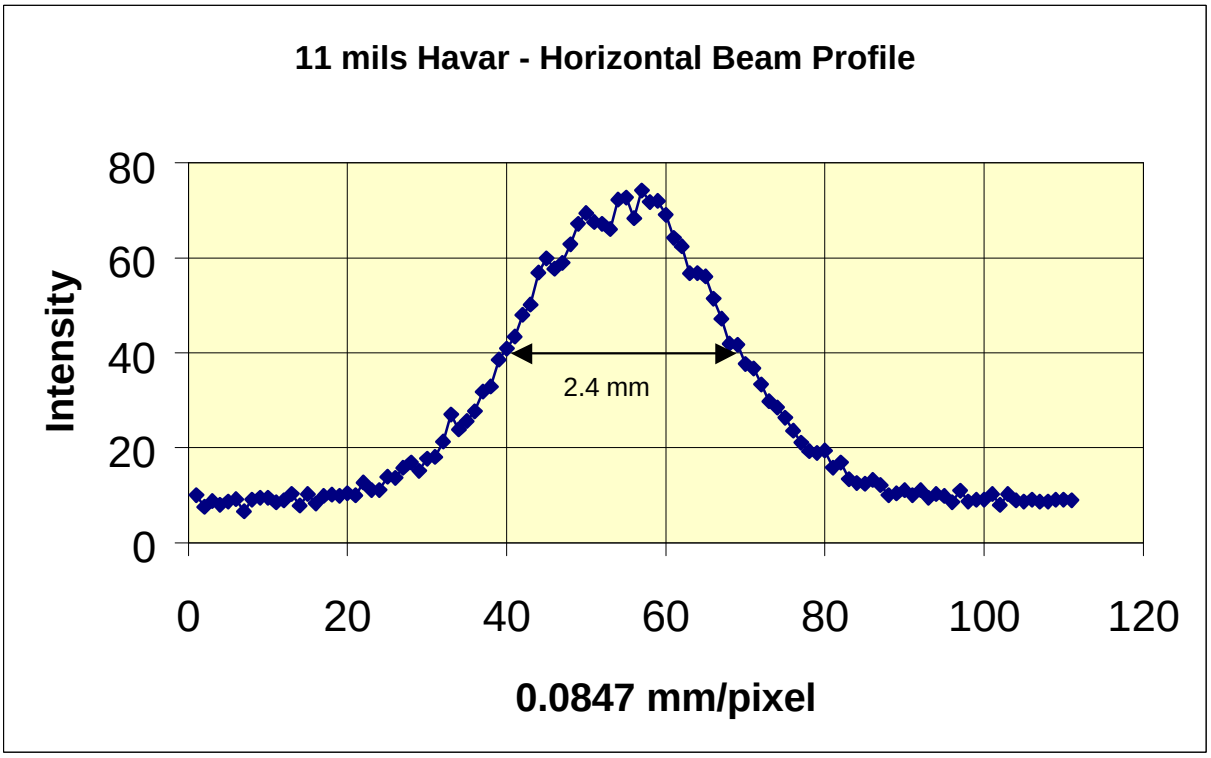

Fig. 9 - Projection on the horizontal axis of the intensity values shown in fig. 8

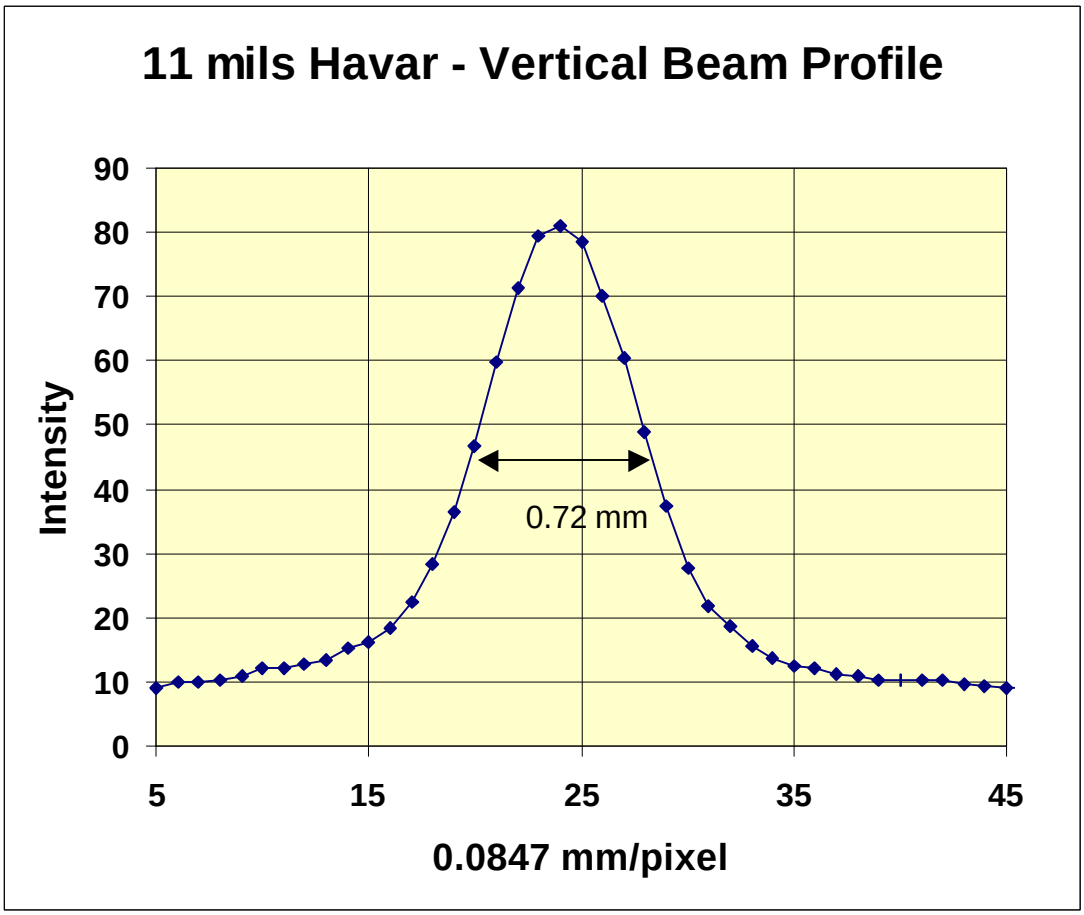

Fig. 10 - Projection on the vertical axis of the intensity values shown in fig. 8

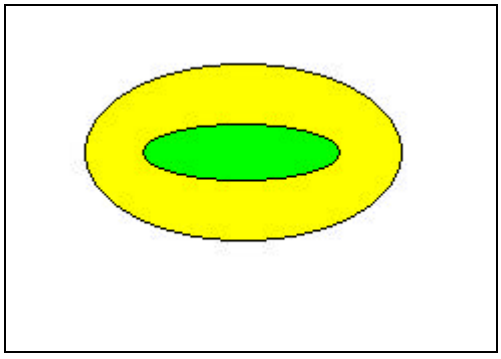

Fig 11 - Beam size determined in the present work (center) as compared to the beam size previously assumed.

Figures 8, 9, 10 and 11 show the results obtained here for the Havar target. We obtain a beam spot area which is about 4.5 times smaller than previously assumed. No correction has been made at this point for the fact discussed before that the source is not in intimate contact with the film. Such a correction leads to an even (slightly) smaller spot. Also the beam position stability, both vertical

and horizontal, must have been extraordinarily good, because any beam motion from shot to shot would enlarge the image.

A second measurement with the Havar target was performed using a 19-day-long exposure and developing all the pictures contained in the Polaroid film pack in order to study the range of the radiations responsible for the exposure and the expected widening of the image due to the increasing distance between the object and the negative (see Fig. 4). Images of diminishing intensity were observed only on the first three pictures. The resulting intensity projections obtained with the same procedures explained above are shown in Figs 12a and 12b.

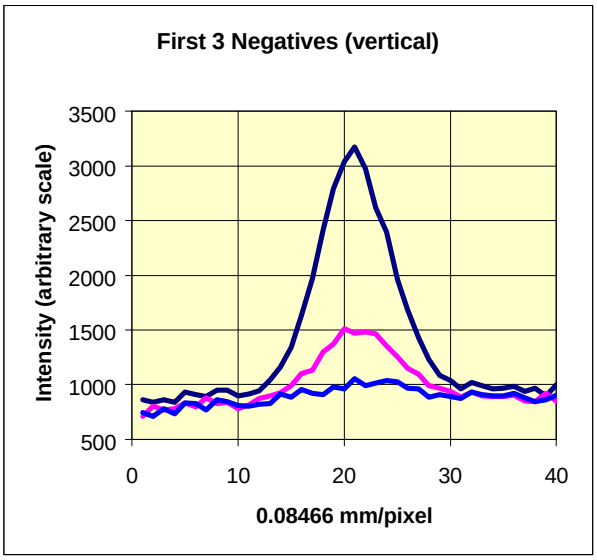

Fig. 12a

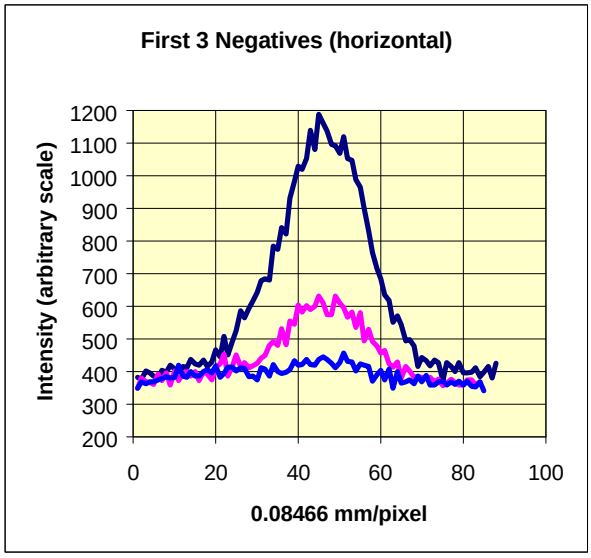

Fig.12b

Table 1summarizes the results of this last measurement with multiple pictures. The indicated errors are estimates.

Table 1. Results for the second measurement with the 11 mil Havar target

	Upper Negative	Second Negative	Third Negative
Vertical width at 1/2 max. (mm)	0.67 ± 0.03	0.72 ± 0.04	0.76 ± 0.05
Horizontal width at 1/2 max (mm)	2.0 ± 0.1	2.7 ± 0.3	
Relative intensities	1	0.36 ± 0.02	0.11 ± 0.02

We see evidence of some broadening of the image as we look at negatives further removed from the target. This broadening for the vertical profile appears to be roughly 0.04 mm per layer. For the horizontal profile the errors are too large to reach any conclusion. One can use this result to correct the vertical width extrapolating to zero distance (see Fig. 4) and this results in a reduction of ~ 6% in the vertical beam size.

The observed, approximately exponential absorption with a mass attenuation coefficient of about 73 cm^2/g, may indicate that the main radiation component producing the image are low energy X-rays.

Further evaluation is difficult because we don't know the chemical composition of the negative material. For an atomic number close to 6 (carbon) we would estimate an X-ray energy of about ~ 4 KeV no too far, e.g., from the ~5.3 K-X rays in Chromium, one of the components of Havar. On the other hand, internal conversion electrons ~250 KeV can not be ruled out either. For the present measurements the nature of the radiation is of no great importance.

Averaging the two measurements with the Havar target and applying the above mentioned 6% correction to the vertical width we obtain the following values for the beam spot dimensions:

Table 2. Averaged and corrected result for the Havar target

Vertical width at 1/2 max. (mm)	0.65 ± 0.03
Horizontal width at 1/2 max (mm)	2.2 ± 0.2

Next we will compare the values of Table 2 with values estimated from the known beam parameters and ion optics of the A3 beam line. Important input for these estimates include:

Proton beam parameters:

Energy 24 GeV
Momentum: 25.5 GeV/c
$\beta \times \gamma$**:** 27.2
dp/p: 0.15 %

invariant horizontal emittance: 90 pi mm-mrad (measured)
invariant vertical emittance: 40 pi mm-mrad (measured)

β_x function at target: 0.4 m (calculated)
β_y function at target: 0.3 m (calculated)
Dispersion at target: 0.5 m (calculated)

Given these beam parameters we calculate the beam spot sizes to be:

σ_y = 0.30 mm $FW_{1/2max}$(vertical) = 0.71 mm
σ_x = 0.90 mm (0.5 from betatron; 0.75 from dispersion) $FW_{1/2max}$(horizontal) = 2.12 mm

These values are in good agreement with the measured values (see table 2)

Comparisons of MARS energy deposition estimates for mercury for experiment E951, and for the 1 MW and the 4 MW options are shown in Figs. 13, 14 and 15. For the simulation of the experiment we used the beam size values of Table 2. The vertical scale of Fig.13 represents energy density values averaged for all angles around the Z-axis. However, at Y=0 no averaging is required and these maximum energy density values are then replotted in Fig. 15. For the 1 MW option we used the Study II values $\sigma_x = \sigma_y = 1.5$ mm for the incident beam width.

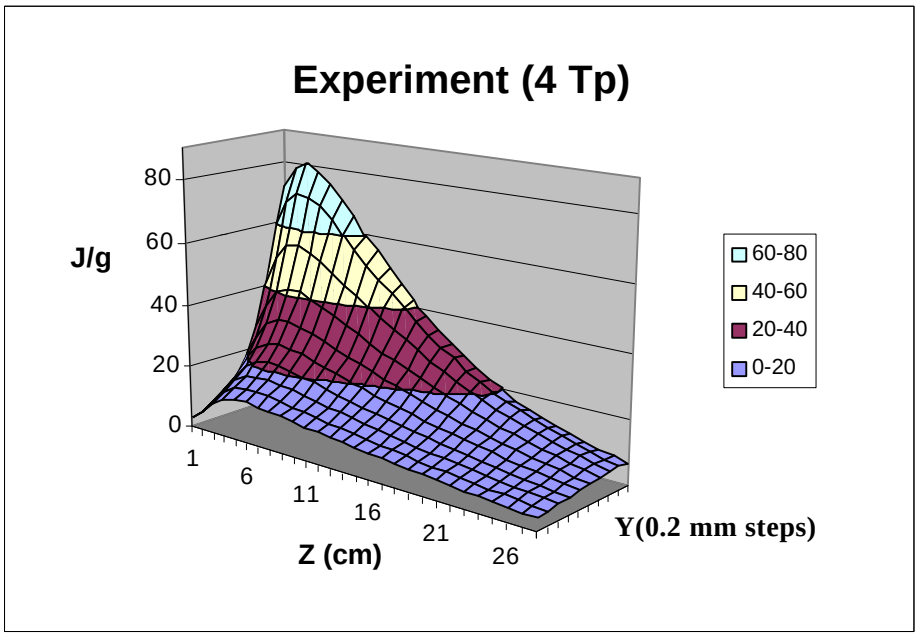
Experiment (4 Tp)
J/g
80
60
40
20
0
1
6
11
16
21
26
Z (cm)
Y(0.2 mm steps)
60-80
40-60
20-40
0-20

Fig. 13

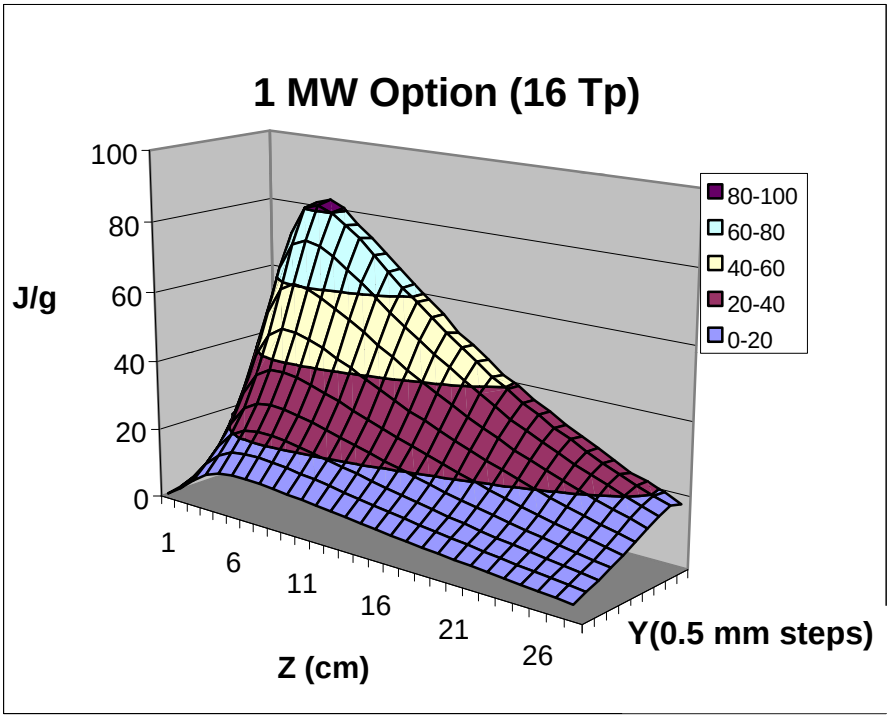
1 MW Option (16 Tp)
J/g
100
80
60
40
20
0
1
6
11
16
21
26
Z (cm)
Y(0.5 mm steps)
80-100
60-80
40-60
20-40
0-20

Fig. 14

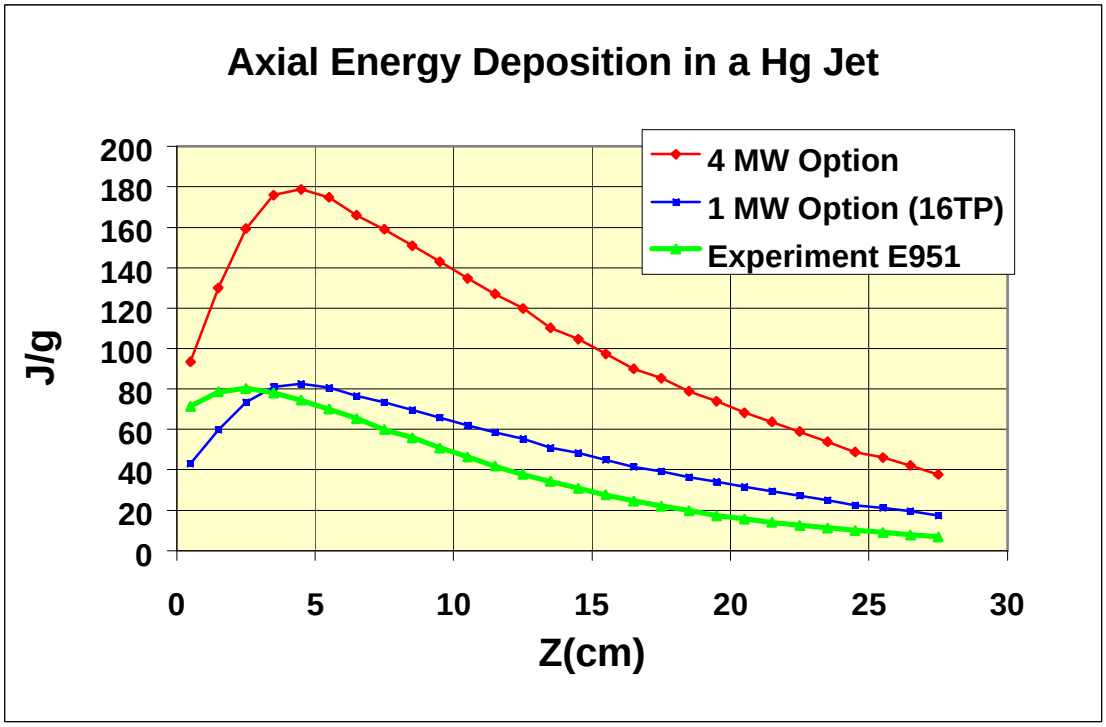

Fig. 15

As we can see in Fig. 14, the estimated maximum energy density deposition for the 1 MW option is 82 J/g, while we estimate that 80 J/g were reached during the experiment. We conclude that values of maximum energy density deposition in mercury close to the ones expected for the 1 MW options were reached during experiment E951. This was achieved with a beam intensity about four times smaller, and an incident beam cross sectional area about 8.7 times smaller than in the final system. The resulting effects, however, can be expected to be a function not only of this maximum energy density, but also of the maximum energy per unit length deposited in the mercury jet, which will be four times larger for the 1MW option as compared to the present experiment, and eight times larger for the 4 MW option.